# Journal Pre-proof


Transitions of lithium occupation in graphite: A physically informed model in the dilute lithium occupation limit supported by electrochemical and thermodynamic measurements

Michael P. Mercer, Manuel Otero, Miriam Ferrer-Huerta, Agustín Sigal, Daniel E. Barraco, Harry E. Hoster, Ezequiel P.M. Leiva

PII: S0013-4686(19)31645-7

DOI: https://doi.org/10.1016/j.electacta.2019.134774

Reference: EA 134774

To appear in: *Electrochimica Acta*

Received Date: 7 June 2019

Revised Date: 8 August 2019

Accepted Date: 26 August 2019

Please cite this article as: M.P. Mercer, M. Otero, M. Ferrer-Huerta, Agustí. Sigal, D.E. Barraco, H.E. Hoster, E.P.M. Leiva, Transitions of lithium occupation in graphite: A physically informed model in the dilute lithium occupation limit supported by electrochemical and thermodynamic measurements, *Electrochimica Acta* (2019), doi: https://doi.org/10.1016/j.electacta.2019.134774.

# Transitions of lithium occupation in graphite: a physically informed model in the dilute lithium occupation limit supported by electrochemical and thermodynamic measurements

Michael P. Mercer[*,1,2,3], Manuel Otero[4,5], Miriam Ferrer-Huerta[1,3,**], Agustín Sigal[4,5], Daniel E. Barraco[5], Harry E. Hoster[1,2,3], Ezequiel P.M. Leiva[4]

[1] Department of Chemistry, Lancaster University, Bailrigg, Lancaster, UK

[2] ALISTORE European Research Institute CNRS FR 3104, Hub de l'Energie, Rue Baudelocque, 80039 Amiens, France

[3] The Faraday Institution, Quad One, Harwell Science and Innovation Campus, Didcot, UK

[4] Departamento de Química Teórica y Computacional, Facultad de Ciencias Químicas, INFIQC-CONICET, Universidad Nacional de Córdoba, Córdoba, Argentina

[5] Facultad de Matemática, Astronomía, Física y Computacíon, IFEG-CONICET, Universidad Nacional de Córdoba, Córdoba, Argentina

***Corresponding author e-mail:** m.mercer1@lancaster.ac.uk

***Corresponding author address: Department of Chemistry, Lancaster University, Bailrigg, Lancaster, UK**

**Dedication:** This paper is dedicated to Prof. Rachid Yazami from Nanyang Technological University on the occasion of his 66th birthday and in recognition of his contributions to graphite electrodes and entropy measurements.

**Abstract:** Understanding the role of the phase transitions during lithiation and delithiation of graphite remains a problem of fundamental importance, but also practical relevance owing to its widespread use as the anode material in most commercial lithium-ion cells. Previously performed density functional theory (DFT) calculations show a rapid change in the lithium-carbon interaction at low occupation, due to partial charge transfer from Li to C. We integrate this effect in our previously developed two level mean field model, which describes the Stage I – Stage II transition in graphite. The modified model additionally describes the most predominant transition that occurs at low Li content in graphite, which results in a previously unexplained feature in voltage and dQ/dV profiles, and thermodynamic measurements of partial molar enthalpy. In contrast with the Stage I-Stage II transition, this extra feature is not associated with observable features in the partial molar entropy and our model demonstrates why. There is a sharp change in the open circuit voltage at very low Li occupation, followed by a transition to a voltage plateau (peak in dQ/dV). The behaviour arises due to the contrasting effects of the partial molar entropy and enthalpy terms on the partial molar Gibbs energy and hence cell voltage. Hence the voltage profile and phase transitions can be approximated for all lithium occupations, potentially allowing a predictive capability in cell level models.

**Keywords:** thermodynamics, lithium ion, graphite, staging, modelling

****Present author affiliation:** Quantum Materials and Sensors, National Physical Laboratory, Teddington, Middlesex TW11 0LW, UK

## 1. Introduction

The use of graphite as the anode in lithium-ion batteries is ubiquitous and the properties of this material have been the subject of extensive research, both from the experimental and the theoretical viewpoints. Recent theoretical work shows that some aspects of the behaviour of this material upon lithiation and delithiation still remain puzzling. For example, the role that the different stages formed play in the entropic behaviour of this material has been recently recognised, in terms of order/disorder transitions [1-5]. Furthermore, the understanding of the occurrence of defective (Daumas-Herold) structures on the basis of the kinetics of the lithium insertion process has also been reached in recent times [6-8].

There has been much interest in describing the staging phenomena, although there is still much room for further important model development. In addition to fundamental understanding, these phenomena are important for achieving a cell level picture for practical applications such as battery management and aging. In our recent and ongoing work, we described order disorder transitions, including the Stage I-Stage II transition, through Grand Canonical Monte Carlo simulations [1, 9–11] and a two level, mean field approach [2, 12]. This transition is responsible for the main step in voltage with respect to lithium occupation (state of charge) that occurs close to 50 % lithiation in graphite.

For further model development and experimental validation, a better understanding of the changes observed at dilute lithium occupation ($0 < x < 0.1$, where $x$ = lithium occupation) is important. Not only do higher order stages (dilute Stage II, Stage III and Stage IV) occur [8, 13–19], but an additional step in the voltage profile occurs at very low ($x < 0.1$) occupation, giving rise to an additional peak in incremental capacity analysis ($dQ/dV$) measurements, which has not yet been explained. These dilute transitions are important, not only to achieve a fundamental understanding of the entire voltage profile, but also the effect of cycling in the low Li occupation region on

graphitic surface structural damage has been appreciated [7, 20], i.e. conditions experienced during deep discharge of a full Li-ion cell.

The goal of the present work is to present a physically informed and useful model, extending our previously successful descriptions of the Stage I - Stage II transition in graphite to include the main transition in the dilute lithium occupation limit, $0 < x < 0.1$. We show, from comparing models with electrochemical and thermodynamic measurements of partial molar entropy and enthalpy, that this transition has a distinct physical origin from the previously reported higher order staging phenomena. In contrast to those effects, which emerge from Li-Li interactions, our model suggests a non-linear change in the interaction between Li and the graphite host lattice at low Li occupation, in contrast with the usual assumption that this interaction term remains fixed with respect to occupation. Accounting for this effect results in the experimentally observed steep change in cell voltage for $x < 0.05$ and the plateau at low Li occupation, $x \approx 0.07$. This model is also supported by early studies of Dahn et al. on the density of states in graphite [15].▪

The paper is organised as follows. In section 2.1 we introduce the experimental methods used to validate the model, i.e. galvanostatic methods, d$Q$/d$V$ and entropy profiling. The latter has also been used to obtain information about the partial molar enthalpy. Experimental results from those methods are presented in section 3.1. Our previously developed two layer Bragg-Williams model is summarised in section 3.2. Physical arguments concerning the change in the Li-substrate interaction at low occupation resulted in an extension to the Bragg-Williams model to include this effect. Modelled output of the electrochemical and thermodynamic profiles dependent on the interaction parameters in the model is shown in section 3.2.2. The experimental and simulated data are drawn together in section 3.3 to determine the interaction parameters. Finally, a rational physical interpretation of the observed features in the relevant profiles is presented in the same section.

## 2.1. Experimental Methods

### 2.1.1. Electrochemical measurements

The carbon working electrode was prepared by a mixture of graphite powder (particle size < 20 μm, synthetic, Sigma-Aldrich), Super P carbon and polyvinylidene fluoride (PVDF) in N-methyl-2-pyrrolidone (NMP) in a mass ratio of 80:10:10, respectively. The slurry was then coated onto copper foil and dried to make the electrode. The electrode consisted of a 8 mm diameter disc, containing 0.86 mg of graphite. 3 electrode Swagelok T cells were used for the measurements, with metallic Li as the counter and reference electrodes, fiberglass as separator and a 1 M $LiPF_6$ in a 1:1 wt/wt mixture of ethyl carbonate (EC) and dimethyl carbonate (DMC) electrolyte.

Measurements were performed on an Autolab PGSTAT302N potentiostat. Three galvanostatic charge-discharge cycles were performed at a current density of 20 $\mu A/cm^2$ (11.68 mA/g, per unit mass of active material), with the fixed voltage limits being between 0.050 and 1.500 V. Cyclic voltammetry was performed at a scan rate of 1 μV/s between 0.005 and 3.000 V.

### 2.1.2. Entropy and enthalpy profiling

CR2302 coin cells, with 16 mm diameter Li foil disk as counter and reference electrode, 12 mm diameter working electrode, Celgard separator and same electrolyte of section 2.1.1 were assembled for the purpose. The carbon working electrodes were assembled as in section 2.1.1 but in a mass ratio of active material, conductive carbon and PVDF binder of 93:3:4, respectively. Coatings onto copper foil with an approximate thickness of 80-90 μm were produced by calendaring.

Experimental measurements for entropy profiling were performed as described in our previous work [12], [22]. The setup comprised an aluminium heat exchanger, in direct thermal contact with the coin cells, which was connected to a Julabo F12 refrigerated – heating circulator, allowing

precise control over the temperature. The temperature was monitored by type-J thermocouples connected to the heat exchangers. For high resolution voltage and temperature measurement a Keysight 34972A data acquisition system with an equipped multiplexer unit was used. The cell current and voltage during the experiment was controlled by a Basytec CTS cycler.

Entropy change measurements were preceded by 3 galvanostatic cycles between 0.020 and 1.500 V at a current density of 37.2 mA/g (C/10, where C = 372 mAh/g, i.e. the theoretical capacity of $LiC_6$) under a controlled temperature of 25 ºC, to ensure stable solid electrolyte interphase (SEI) formation and to validate the electrochemical behaviour. We separately verified that the galvanostatic results from the coin cells at constant temperature gave comparable results to the three electrode cell measurements as described in section 2.1.1. The cells were then charged under a constant current-constant voltage condition to 1.500 V at 14 mA/g (C/25) at 28 ºC followed by holding the voltage constant at 1.500 V for at least one hour. Entropy profiling was then performed in an iterative procedure, where the current and temperature were changed dynamically as outlined in Table 1. Each iteration was repeated until the cell voltage was less than 0.005 V, corresponding to 75 steps in total. State of charge, *x*, was obtained from normalising the change of capacity from each galvanostatic step in Table 1 to the total change of capacity obtained during the entire experiment.



Table 1. Experimental parameters of the entropy change measurements

| **Step** | **Time (min)** | **Temperature (ºC)** |
|---|---|---|
| Discharge (C/25) | 20 | 28 |
| Open circuit voltage (OCV) relaxation | 20 | 28 |

| | | |
|---|---|---|
| Temperature step $T_1$ (OCV) | 20 | 25 |
| Temperature step $T_2$ (OCV) | 20 | 22 |
| Temperature step $T_3$ (OCV) | 20 | 28 |

The procedure is very similar to galvanostatic intermittent titration technique (GITT), where the constant current and OCV steps are alternated. Here, similarly to our previous work [12, 22], the gradient of the change in OCV with temperature between the first OCV relaxation and temperature step $T_2$ was used to determine the partial molar entropy, $\Delta S$, i.e.

$$\Delta S = \left(\frac{\partial S(x)}{\partial x}\right)_{p,T} = \left(\frac{\partial E_{OCV}(x)}{\partial T}\right)_{p,x}, \qquad (1)$$

and hence the partial molar enthalpy, $\Delta H$, was determined by

$$\Delta H = \Delta G + T\Delta S = -F\left(E_{OCV}(x) - T\left(\frac{\partial E_{OCV}(x)}{\partial T}\right)_{p,x}\right), \qquad (2)$$

where $\Delta G$ = partial molar Gibbs energy, $x$ = fraction of lithium intercalated in the electrode with respect to the maximum capacity ($0 < x < 1$), $E_{OCV}(x)$ = open circuit voltage (OCV), T = absolute temperature, $p$ = pressure, $F$ = Faraday constant. The protocol was designed so that the central temperature during the OCV relaxation was 25 ºC, to facilitate comparisons with the electrochemical measurements. To minimize the possible effects of thermal drift we used our previously developed open circuit voltage (OCV) fitting and drift subtraction algorithms, described in detail by Osswald *et al.* [22], and the thus obtained OCV was used in equations 1 and 2 to obtain $\Delta S$ and $\Delta H$, respectively.

3.1. Experimental results

3.1.1. Electrochemical results

Electrochemical results, showing the variation of the voltage with time are shown in Figure 1a. These results correspond to the third galvanostatic cycle: results from the very first cycle, i.e. the solid electrolyte interphase (SEI) formation are shown in the supplemental information, Figure S1. The results from the third cycle show a stable and repeatable behaviour. From numerical differentiation of these results, shown in Figure 1b, dQ/dV analysis was obtained. Plateaux in Figure 1a correspond to the labelled peaks in Figure 1b.

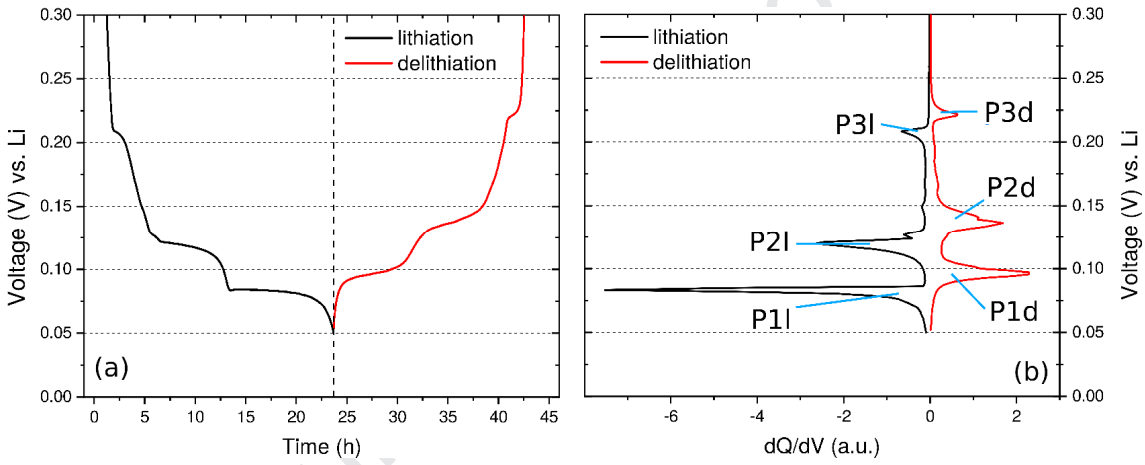


*Figure 1. (a) Variation in the cell voltage with time, from the 3rd galvanostatic cycle conducted at 11.68 mA/g . (b) dQ/dV analysis, obtained through numerical differentiation of the results shown in (a). Details of the labelled peaks are described in the main text.*

The pair of peaks P1d/P1l and P2d/P2l arise from an order/disorder transition, as modelled in our previous work [2, 3]. Additionally, there is an extra plateau in the voltage profile, Figure 1a, at about E = 0.21 V, showing a deviation from ideal solid solution (Nernstian) behaviour. This gives rise to two additional peaks P3l/P3d in the dQ/dV profiles of Figure 1b. This behaviour is also observed in slow rate cyclic voltammetry (SRCV) experiments, shown in Figure S2. By integration, we obtained a fractional coverage of 0.07 under P3l/P3d, from SRCV and d*Q*/d*V*. Peak coverages,

normalised to the total charge passed during the respective cycle, are shown in Table 2. The results are in good qualitative agreement with those of Aurbach et al. [23, 24]▪ .

*Table 2. Fractional coverage obtained from integration of the charge corresponding to the peaks highlighted in Figure 1b (galvanostatic) and slow rate cyclic voltammetry (Figure S2).*

| Lithiation | | | Delithiation | | |
|---|---|---|---|---|---|
| Peak | Galvanostatic | Voltammetry | Peak | Galvanostatic | Voltammetry |
| P1l | 0.52 | 0.56 | P1d | 0.51 | 0.54 |
| P2l | 0.41 | 0.37 | P2d | 0.42 | 0.39 |
| P3l | 0.07 | 0.07 | P3d | 0.07 | 0.07 |

The coverage obtained from P3l/P3d does not correspond to an integer fraction (e.g. 0.33, 0.25) as would be expected for a transition to a higher order stage such as Stage III or Stage IV [13]. The origin of this peak has not previously been completely explained and the subsequent analysis provides clarification. Since the occupation values from peaks P3l and P3d are indistinguishable within the limit of experimental error, we will use the variable $\theta_{P3}$ in the subsequent text to refer to their occupation values synonymously.

We note that the difference between the charge and discharge behaviour shown in Figure 1a-b has been previously observed [5]. The goal of the present work is to provide a physical model to describe the three major transitions: P1l/P1l, P2l/P2d and P3l/P3d, with a particular emphasis on the physical interpretation of the latter peak, P3l/P3d.

3.1.2. Thermodynamic measurements of partial molar enthalpy and entropy

Additional insight into the transitions can be obtained through examination of experimental entropy profiles and enthalpy profiles, which are shown in Figure 2a. Results for the partial molar entropy are in good agreement with those of Reynier et al. [4, 25-26], Thomas and Newman [27] and Allart et al. [5]. The main features in the enthalpy profiles, i.e. the flat line for $x > 0.5$, step at $x = 0.5$, broad peak at x= 0.25, and sharp decrease for $x < 0.05$, have previously been reported [25, 27]. Due to the higher data collection rate than previous work we can resolve an additional peak at about x = 0.05 that has not previously been reported and is predicted within our model.

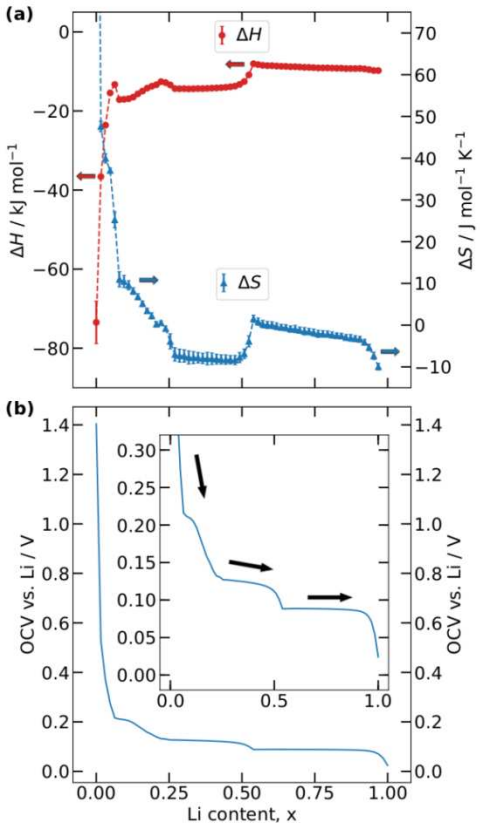


*Figure 2. (a) Enthalpy and entropy profiles from Li/graphite half cells (partial molar enthalpy: left axis, partial molar entropy: right axis, as indicated by arrows). (b) Open circuit voltage (OCV) values obtained from the entropy profiling procedure. Inset shows the same profile over a narrower potential window.*

Entropy profiles, shown in Figure 2a, display a transition at approximately $x$ = 0.5, which is the order/disorder transition associated with the Stage I – Stage II transformation [2, 4, 11, 25-26]. Although higher order stages (dilute Stage II, Stage III and Stage IV) have previously been measured in electrochemical experiments at lower Li content, $x < 0.5$ [13, 28], and identified in Li-C compounds synthesised through heat treatment [18], these stages do not result in well defined transitions in the entropy profiles [25, 27]. In fact, the result for $x < 0.25$ shown in Figure 2a approximates well to the monotonic drop in partial molar entropy expected for ideal solid solution filling. This observation appears to be at odds with the voltage profile and dQ/dV results, Figure 1a-b, showing an extra peak and plateau, respectively, at low Li occupation.

The enthalpy profile shows a sharp transition in the dilute Li occupation limit. The change observed in the partial molar enthalpy is dramatic: as the occupation $x$ increases from 0.00 to 0.05, partial molar enthalpy $\Delta H$ increases from -74 kJ $mol^{-1}$ (-0.77 eV) to -15 kJ $mol^{-1}$ (-0.17 eV). Thus, while the partial molar entropy resembles the behaviour of an ideal lattice gas for $x < 0.25$, the partial molar enthalpy indicates that drastic changes take place in the energetics of the system at low Li occupation. We also observe a sharp peak in $\Delta H$ at approximately $x = 0.05$, which was not clearly resolved or explained in previous measurements. As we show in the subsequent sections, these phenomena can be modelled by a change in the interaction of Li with the carbon substrate.

The open circuit voltage (OCV) obtained from the entropy profiling procedure, shown in Figure 2b, is in good agreement with previous results [26, 28] and our own galvanostatic data obtained during lithiation from a 3 electrode cell, as shown in Figure 1a. The rapid change in voltage for $x < 0.05$, and the voltage plateau at $E$ = 0.21 V, are associated with the steep change and peak, respectively, in the enthalpy profiles.

We note that there is a broad peak in the enthalpy profile at about x = 0.25, and a correspondingly small shoulder in the entropy profile. The former can be observed in the data of Reynier et al. (Figure 5b, ref. [25], MCMB graphite), but the latter has not been found or remarked upon as far as we know. It is possible that this feature corresponds to a dilute Stage IV transition. However, its influence on the OCV is negligible, as shown in the inset of Figure 2b. Therefore, in the next stage of model development, this feature was neglected in favour of a physically informed description of the three main voltage plateaux, and the steep change in partial molar enthalpy and OCV at low Li occupation. These effects are responsible for much more consequential changes in the electrochemical behaviour. The model and results are described in the subsequent section.

### 3.2. Two layer Bragg-Williams model

#### 3.2.1. Simulation methodology and physical basis

A schematic of our two level Bragg-Williams model is shown in Figure 3. We used this model in our previous work to model lithium insertion in graphite [2, 3] and, in a very similar form, lithium manganese oxide spinel with point defects [12]. All input parameters, along with their meaning and values are tabulated in Table 3.

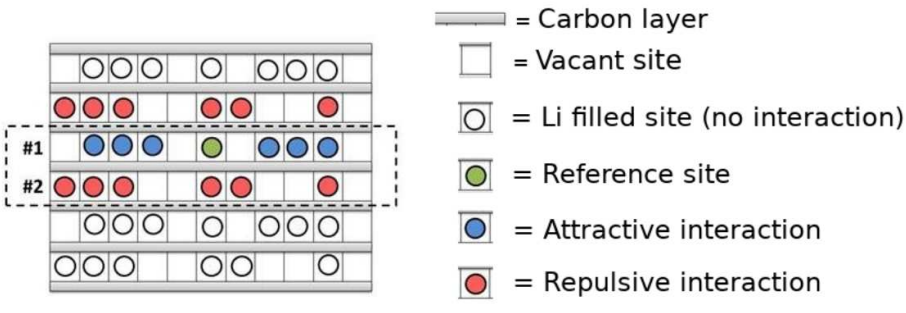


*Figure 3. Schematic illustration of the two level Bragg-Williams model. Pairwise interactions in the same layer (g term) and between adjacent layers (Δ term) are considered, resulting in attractive and repulsive interactions, respectively.*

*Table 3. Definition of input parameters within the model.*

| Parameter | Definition | Value |
|---|---|---|
| T | Absolute temperature | 298 K |
| $E_0$ | Value of the point term in the limit of high occupation | -4.51 kT |
| A | Amplitude of the change in the point term at low Li occupation | varied |
| B | Decay constant for the change in the point term at low Li occupation | varied |
| G | Interaction between Li atoms in the same layer (intralayer interaction) | -0.45 kT |
| Δ | Interaction between Li atoms in adjacent layers (interlayer interaction) | 1.12 kT |
| M | Number of available lattice sites in each layer | 600 |

The model relies on summation of the partition function in a 2 level model

$$Q(N, 2M) = \sum_{i\ states} \exp\left(-\frac{E_i}{kT}\right) = \sum_{j\ levels} \Omega_j \exp\left(-\frac{E_j}{kT}\right), \qquad (3)$$

where $N$ is the number of particles (Li ions) in the system (maximum $N = 2M$), $\Omega_j$ is the number of degenerate energy levels of energy $E_j$, $k$ is the Boltzmann constant, $T$ is the absolute temperature. All the thermodynamic properties of the system may be straightforwardly evaluated by counting the number of configurations for a system of $N = N_1 + N_2$ particles, $N_i$ being the number of particles in slab $i$, as shown in our previous work [3]. In particular, we note that the degeneracy, or number of energetically equivalent configurations, is given by

$$\Omega_j = \frac{(M!)^2}{(M-N+j)!(N-j)!(M-j)!j!}, \quad (4)$$

for each energy level $j$.

The interaction Hamiltonian for each energy level $E_j$ is

$$E_j = E'_0(N_1 + N_2) + \frac{3g\left({N_1}^2+{N_2}^2\right)}{M} + 2\Delta N_1 N_2/M. \quad (5)$$

In conventional lattice gas models the term $E'_0 = E_0$, where $E_0$ is a constant describing the Li-C interaction. It corresponds to the potential value at which the lattice sites are half filled. On the other hand, changes to the shape of the voltage profile with occupation usually arise only from the Li-Li interaction terms, i.e. $g$ and $\Delta$ in this case. As shown in our previous work [2], the model results in well defined peaks, P1d/P1l and P2d/P2l in accordance with the ones obtained experimentally. We previously obtained values $g$ = -0.45 kT and $\Delta$ = 1.12 kT, by comparing the simulation results with the experimental half widths and relative positions of the two peaks from slow rate cyclic voltammetry, Figure S1 [2]. The effective attractive force between lithium atoms in the same layer in our model is in line with the theoretical work of Filhol et al. [29], which shows a minimum in the binding energy of Li as a function of distance between the Li atoms in the same layer, as well as

with previous experimental results [23]. The value of $E_0$ = -4.51 kT was determined by comparing the potential scale of the simulations and the experimental results.

Although simple from a modelling perspective, the commonly made assumption that the point term is constant across the intercalation range may not be justified. Dahn et al. highlighted the fact that, when the Fermi level of an intercalation compound moves through a region with a low density of states, as in a semimetal such as graphite, large changes in chemical potential of the intercalated Li result [21]. Then, the parameter $E_0$ is not constant but changes rapidly with x.

Evidence for deviations from a constant point term $E_0$ during lithiation in graphite can also be found in earlier theoretical work of Di Vicenzo et al. [30], who found that a typical alkali metal donor in graphite creates a screening charge that decays algebraically with an effective screening length λ of about 3.8 Å. For comparison, the screening length of typical metal such as copper is λ = 0.55 Å [30]. Assuming a typical Thomas Fermi screening model [31], we find that while in the second case the screening factor is reduced to 1% of its maximum value at 2.53 Å, for graphite the corresponding distance would be 17.5 Å. This fact has been attributed to the reduced dimensionality of the graphite host. Interestingly, the distance between lithium ions at x = 0.07, during the P3l/P3d process would correspond to an average distance between $Li^+$ ions of 16.1 Å. That is, the occurrence of the associated peak occurs right when the screening of the coulomb forces between inserted ions start to fade. At this point, a way to reduce these repulsive forces would be to reduce the charge transfer from Li to the graphite lattice.

This phenomenon is consistent with a density functional theory (DFT) study of Garay-Tapia et al. [32], who showed that the binding energy of Li to graphene undergoes a rapid transition at low occupation, due to partial charge transfer from Li to the substrate. Moreover, Valencia et al. [33] have found the same trend for the lithium-graphite system. Lee and Persson [34] showed the effect

of an increasing number of carbon layers on the binding energy of Li to the substrate. They determined that, as the number of carbon layers increases from 2 to 8, the energy converges to the same value, with respect to the number of carbon layers, at low Li occupation. Moreover, they determined that the charge transfer between intercalated Li ions and graphene layers is limited to the nearest neighbours. Hence, it is appropriate to use DFT results for Li-graphene to approximate the change in binding energy at very low Li occupation. These results, replotted from Garay-Tapia et al. [32], are shown in Figure 4. The proportion of the charge surrounding the Li atoms is presented in Figure 4a. From $Q_{Li} = 1 - Q_{C,}$ where $Q_C$ is the fraction of the charge surrounding the carbon atoms, $Q_{Li,}$ the fraction of charge surrounding the Li atoms, was determined. Results from their work for the variation of the Li binding energy as a function of occupation are shown in Figure 4b.



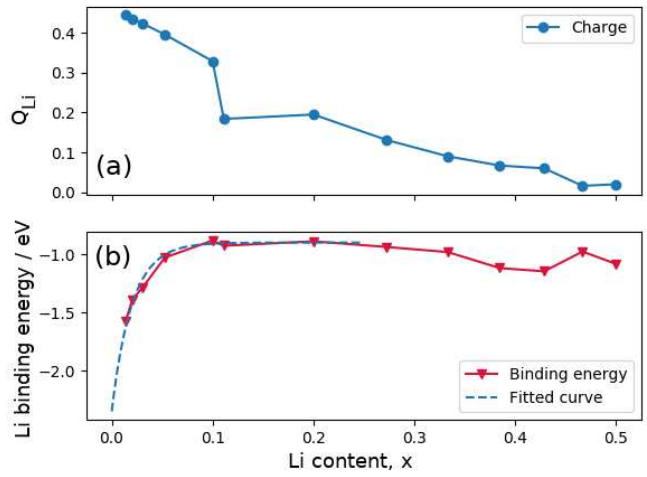


*Figure 4. (a) Variation in the fraction of the charge surrounding the Li atoms ($Q_{li}$) and (b) variation in the binding energy, as a function of the occupation, x. The fitted curve, dashed line in (b), was based on the data points for x < 0.25 only. Input parameters in equation 6 for illustration were* $E_0$ = -35 kT, $\alpha$ = -56 kT, $\beta$ = 50. *Results in (a) replotted based on the lowest energy configurations (centred sites) from Figure 1 and Figure 4 from Garay-Tapia et al.. Results in (b) were obtained from the centred site configurations in Table 2 and Table 4 from Garay-Tapia et al. Reused with*

*permission from A.M. Garay-Tapia et al., J. Chem. Theory Comput. 8 (2012) 1064-1071. Copyright American Chemical Society (2012).*

The results of Figure 4a are also consistent with the calculations made by Rakotomahevitra et. al. for the insertion of a Li impurity in graphite (x→0), where they found that the Li impurity kept a remaining charge of 0.483 $e^-$ [35]. It is important to highlight that the estimation of charge transfer in graphite/lithium systems is very sensitive to the analysis method used, and different values can be found elsewhere [36, 37]. As pointed out in the work of Valencia et al. [33] the same system may present a charge of 0.43 $e^-$ by Mulliken method, 0.47 $e^-$ using Voronoy´s analysis, 0.60 $e^-$ for Löwdin analysis or 1.0 $e^-$ for Bader analysis. Although the numerical values depend on the analysis method, the trend shown in Figure 4a is independent of that method.

The results of Figure 4b suggest a non-linear decay in the total energy as a function of occupation. At the dilute Li occupation end we can neglect Li-Li interactions and approximate the change in total energy from the point term, $E'_0$, only, using an exponential decay relationship, i.e.

$$E'_0 = E_0 + \alpha \exp(-\beta x) \qquad (6)$$

where $E'_0$ is a modified Li-C interaction, $E_0$ is a constant, representing the Li-C interaction outside of the dilute occupation limit, and $\alpha$ and $\beta$ are empirical constants representing the amplitude and decay constant respectively of the change to the Li-C interaction with occupation $x$. For an exponential decay relationship, $\beta > 0$. $\alpha$ and $\beta$ can be correlated with the following physical interpretation. $\alpha$ is related to the magnitude of the Li-C interaction for low occupations. In fact, as x→0, so $E_0' \rightarrow E_0 + \alpha$, so that a negative $\alpha$ indicates that in the limit of low occupations the interaction with the substrate becomes stronger, and conversely for a positive $\alpha$ value. On the other hand, $\beta$ represents how suddenly the Li-C interaction varies with the occupation as the graphite is

progressively occupied by Li ions. The origin of these changes in terms of the band structure of the system has been discussed in detail by Dahn et al. [21]. This picture is consistent with the rapid increase of the partial molar enthalpy in the experimental results of Figure 2a, for $x < 0.05$.

To integrate this effect into our model, a larger number of available insertion sites, $M$, in each layer was required than our previous work [2, 12], which only simulated P1l/P1d and P2l/P2d. This is because of the small range of $x$ over which the P3 transition occurs. Results for $M = 600$ were found to be fully converged with respect to the system size. Calculating the degeneracy, equation 4 was achieved through a modified Stirling approximation (MSA) of the form $\log(n!) = \log\left(\sqrt{2\pi n}\right) + n(\log(n) - 1)$, because the conventional Stirling approximation (SA), $\log(n!) = n(\log(n) - 1)$, was not sufficiently accurate. The numerical accuracy of this approximation was compared with direct evaluation of the factorials in the expressions of the degeneracy with $M = 170$, which was the absolute maximum that could be calculated before numerical overflow errors occurred. For illustration, results obtained within SA, MSA and direct evaluation of the degeneracy factors in equation 4 are shown in Figure S7 for M = 150. The SA (Figure S7a) results in an underestimation of the peak heights and half widths in dQ/dV, whereas results from the MSA (Figure S7b) are indistinguishable from those obtained by directly evaluating the factorials (Figure S7c), confirming the validity of the MSA. Results for the MSA for 100 < M < 300 are shown in Figure S8 and extended to the range 300 < M < 500 in Figure S9. Although the peaks for P1l/P1d and P2l/P2d are nearly indistinguishable with respect to the system size, subtle changes are observed in peak P3 in Figure S8. Increasing the value of M above M = 300 (Figure S9) shows no changes in peak half width or amplitude, confirming that the input value M = 600 is more than sufficient to describe the system behaviour.

3.2.2. Simulation results

The variation of $E'_{0,}$ the term in equation 6 relating to the interaction of Li with the substrate is shown in Figure 5, as a function of voltage and occupation, for different input values of $\alpha$. Output from the electrochemical profiles is shown in Figure 6.

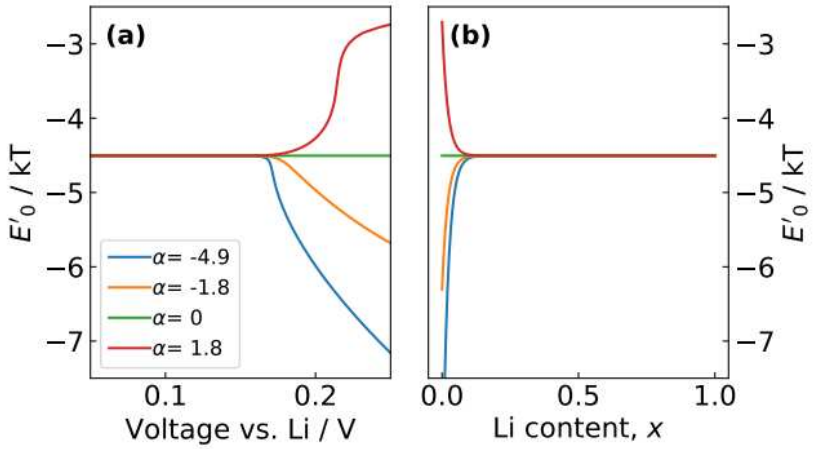


*Figure 5. Variation in the modified Li-C interaction, $E'_0$, as a function of (a) voltage and (b) Li occupation. The value of $\alpha$, in kT, is shown in the legend. The value of $\beta$ was fixed at 50 in the calculation results shown in the figure.*

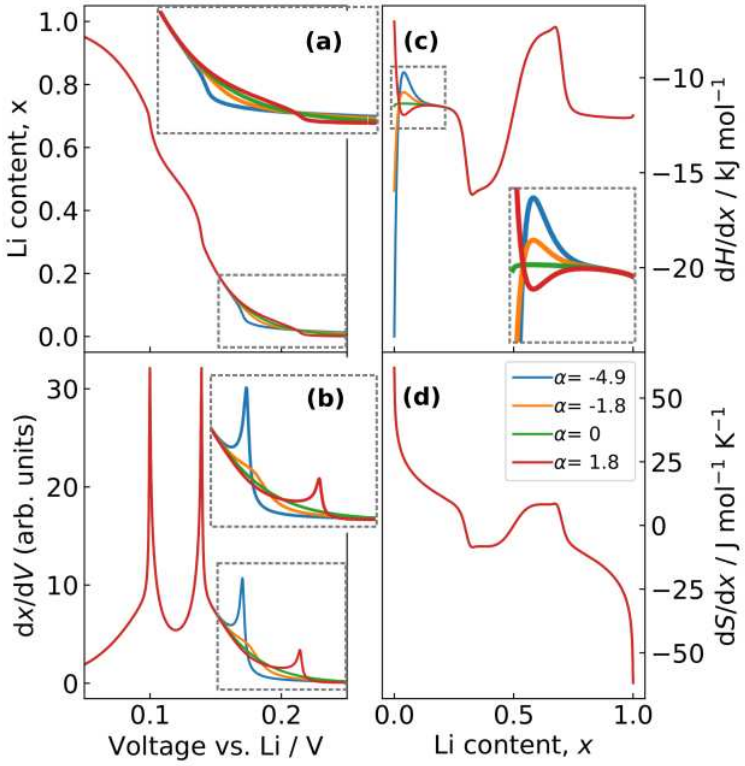


*Figure 6. Simulated results for the variation in (a) lithium content, x, and (b) dx/dV, as a function of the cell voltage, (c) enthalpy and (d) entropy profiles as a function of the lithium content. Profiles correspond to the variation in $E'_0$ shown in Figure 5. Insets (grey dashed lines) show features in finer detail. Value of α, in units of kT, presented in the legend of (d).*

Simulated results close to Li content, x = 0.5, are in good agreement with our previous work [2]. The two voltage plateaux in Figure 6a, and peaks in the dQ/dV, enthalpy and entropy profiles, Figure 6b, 6c and 6d, respectively, arise due to an order/disorder transition because of the Li-Li interactions in the system.

The simulated results show additional features at low Li occupation arising from the change in Li-C interaction, as most clearly shown in the insets of Figure 6a-c. The simulated results for the voltage

profile and dQ/dV response, Figure 6a and Figure 6b, are in good agreement with the respective experimental data, Figure 1a and 1b, when $\alpha \neq 0$. These data show an additional peak resembling P3l/P3d, whose amplitude is related to the absolute value of $\alpha$.

A peak arises from the model when $\alpha < 0$ and $\alpha > 0$, shown in the insets of Figure 6b and 6c. From only dQ/dV it is difficult to determine the sign of the interaction and therefore thermodynamic information from enthalpy profiles can provide additional confirmation. Comparing the simulated enthalpy profiles, Figure 6c, when $\alpha < 0$ with experimental data in Figure 2a shows a similar trend at dilute occupation, providing support for $\alpha < 0$. We note that $\alpha < 0$ is also consistent with the physical arguments presented in section 3.2.1 and the DFT data in Figure 4b. On this basis, we disregard the solutions for $\alpha > 0$. When $\alpha < 0$ the host lattice becomes less attractive to Li as the occupation increases and stabilises to a constant, as shown in Figure 5a-b.

The small peak observed in the enthalpy profile is consistent with a similar feature in the experimental data, Figure 2a when $\alpha < 0$. The enthalpy term associated with this interaction, $H_{\text{substrate}}(x)$, excluding effects from the Li-Li interactions, is related to the interaction term $E_0'(x)$

$$H_{substrate}(x) = E_0'(x)x, \qquad (7)$$

and so inserting equation 6 into equation 7 the partial molar enthalpy term from only the substrate is given by

$$\left(\frac{\partial H_{substrate}(x)}{\partial x}\right)_{p,T} = \Delta H_{substrate} = \alpha(1-\beta x)\exp(-\beta x), \quad (8)$$

as shown in further detail the supplemental information. Equation 8 results in a clearly defined maximum in the partial molar enthalpy. This maximum is responsible for peak P3, in the experimental data and simulations, for reasons that are explained further in section 3.3.

We found that behaviour resembling a first order phase transition results from this model when the amplitude of $\alpha$ is large, i.e. $\alpha$ < -6 kT. The onset of this transition was found to be independent of the value of $\beta$. However, we note that the experimental dQ/dV results in Figure 1b do not show sharp discontinuous peaks P3l and P3d, which would be associated with the onset of a first order phase transition and a concomitant transformation to a two phase coexistence regime. On this basis we consider only -6 kT < $\alpha$ < 0 *kT*.

Regardless of the sign of $\alpha$, the varying point term $E'_0$ does not result in any change to the entropy profiles as a function of $x$, as shown in Figure 5d. This is supported by the experimental result of Figure 2a, showing only a monotonic change in partial molar entropy in the region $0 < x < 0.25$. This observation that will be picked up in further detail in section 3.3. Note that this behaviour results from the low occupation under the peak, well before the onset of the Stage I – Stage II transition, and the fact that $E'_0$ is proportional to the overall occupation x, rather than the occupations of the individual layers, $N_1$ and $N_2$ (as in the case of the interaction terms $g$ and $\Delta$).

In general, the simulated results support a different origin of peak P3l/P3d to that of the other peaks, P1l/P1d and P2l/P2d. While the latter peaks emerge from the Li-Li interactions present in the system, causing pronounced entropy profile features, P3l/P3d does not behave like an order/disorder transition. In the low Li occupation region, the profiles approximate to an ideal solid solution on a voltage scale distorted by a change in the interaction of Li with the substrate, based on the physical arguments in section 3.2.1.

3.3. Evaluation of parameters by comparing simulated and experimental results

Through quantitative comparison with experimental dQ/dV data, we can quantify values of the coefficients, α and β, in equation 6. Relationships for dQ/dV for variable α and β, as a function of x, are shown in Figure 7. Results from the two layer model are presented in Figure 7a-b. We derived analytical expressions to describe a Langmuir isotherm with an $E'_0$ term modified according to equation 6. Full details of the derivation are presented in the supplemental information. The key relationship is that the electrochemical potential, $E(x)$, of the modified Langmuir isotherm is

$$E(x) = -E_0 + \alpha(1-\beta x)\exp(-\beta x) + kT(\log(x) - \log(1-x)), \quad (9)$$

where peak P3l/P3d arises from the extra factor of $(1 - \beta x)$ present in the partial molar enthalpy term (c.f. equation 8), giving rise to the small peaks observed in Figure 5c, and observed experimentally in Figure 2a. The entropic term $kT(\log(x) - \log(1-x))$ is the same as the one from the Langmuir isotherm, $E_{Langmuir}$

$$E_{Langmuir}(x) = -E_0 + \alpha(1-\beta x)\exp(-\beta x) + kT(\log(x) - \log(1-x)). \quad (10)$$

We define the difference, $D(x)$, between the modified and standard Langmuir isotherms as

$$D(x) = E(x) - E_{Langmuir}(x) = -\alpha(1-\beta x)\exp(-\beta x). \quad (11)$$

In terms of output, we verified that this approximation is equivalent to taking the two layer model with input parameters $g = 0$ and $\Delta = 0$, as shown in supplemental Figure S3-S6. The utility of this approximation is based on the observation that the partial molar entropy, as a function of $x$, does not depend on $\alpha$ or $\beta$ as shown in Figure 6d. As a consequence, the formation of peak P3l/P3d is not

substantially affected by the presence of the Li-Li interactions in the system. This allowed us to evaluate the position of the P3l/P3d peak maximum, $x_{0,}$ over a wide range of $\alpha$ and $\beta$ values using equations 9-11. Results from the thus modified Langmuir isotherm are presented in Figure 7c-f.

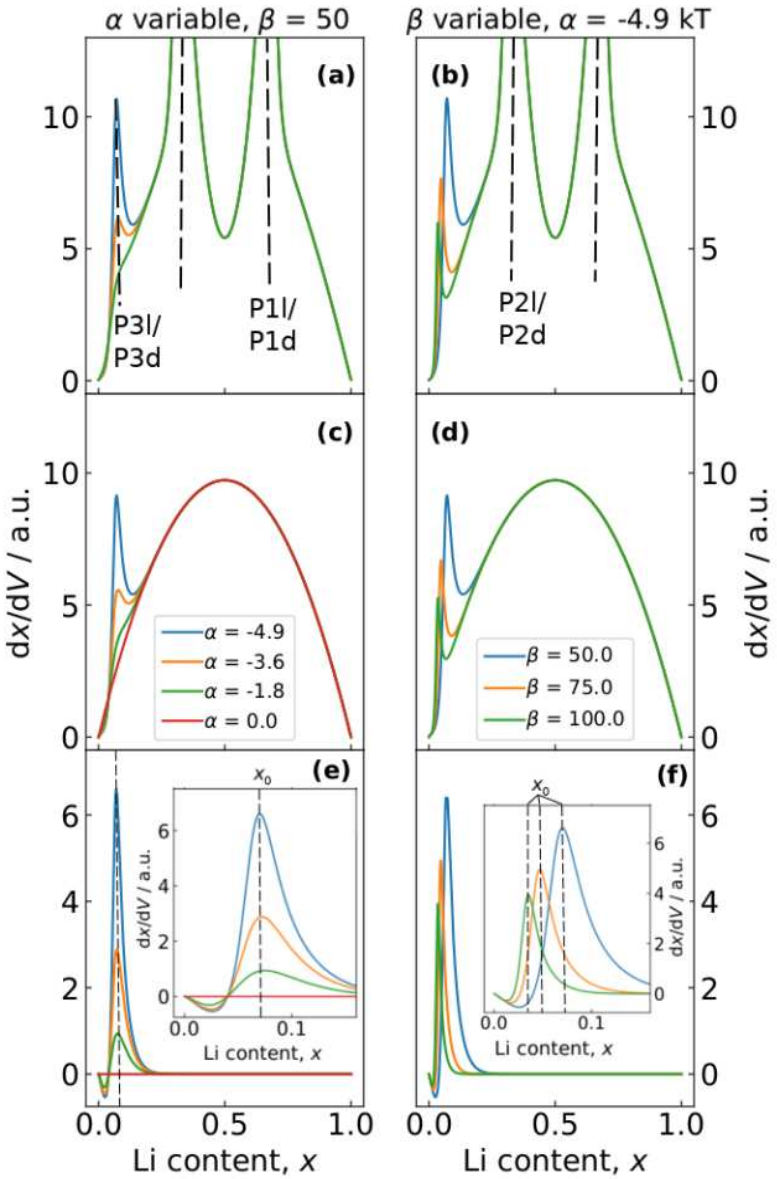


*Figure 7. Results for dx/dV plotted as a function of occupation, x. (a),(b): two layer Bragg-Williams model with point term correction. (c),(d): results from analytical approximation to Langmuir isotherm with point term correction. (e),(f) result of subtracting profiles (c),(d) from the uncorrected*

*dx/dV result from the Langmuir isotherm (red line in graph (c)). Inset of (e) and (f) shows the same data over a narrower x range.*

Comparing Figure 7a with 7c, and Figure 7b with 7d, confirms that the relative positions and magnitudes of peak P3l/P3d are not significantly affected by the presence, or absence, of the order/disorder transition peaks P1l/P1d and P2l/P2l. This fact is consistent with the insensitivity of the partial molar entropy over the relevant range of α and β values (c.f. Figure 6d).

To evaluate the change in occupation corresponding to peak P3, we subtracted the dx/dV result obtained from the modified Langmuir isotherm, described by equation 9, from the same result arising from the standard Langmuir isotherm ($\alpha = 0$), described by equation 10. This is equivalent to taking D(x) as defined in equation 11 and numerically differentiating the result. These results are shown in Figure 7e-f. The evolution of the peak P3l/P3d maximum position, $x_{0,}$ is shown in the insets. Figure 7e shows that $x_{0,}$ is virtually independent of the value of $\alpha$ when $\beta$ is fixed. A much greater variation of $x_0$ is found with respect to $\beta$ as shown in the right hand column of Figure 7.

We use $2x_0 \approx \theta_{P3}$ ($\theta_{P3}$ = experimental peak P3l/P3d coverage = 0.07) to obtain values of $\alpha$ and $\beta$ from the experimental peak coverages $\theta_{P3}$, based on the approximate symmetry of the peaks. Since the model contains two unknown parameters, $\alpha$ and $\beta$, it is impossible to uniquely determine their values just by comparing the simulated and experimental values of $x_0$ and $\theta_{P3}$. As a final indicator of these values, we can also compare the full width half maximum (FWHM) of the experimental and simulated peaks, for all values where $2x_0 = \theta_{P3}$. This value gives an indication of whether the effective interactions in the system are attractive or repulsive; a half width < 90 mV is usually assigned to attraction while FWHM > 90 mV is correlated with repulsion [3]. Although the

computed value of FWHM = 5.8 mV suggests an apparent attractive interaction within the system, the competing influences of the partial molar entropy and enthalpy in this occupation region require further explanation as we shall show subsequently. Input parameters consistent with the experimentally determined $x_0$ and FWHM were $\alpha$ = -4.9 kT and $\beta$ = 106, as shown in Figure 8.

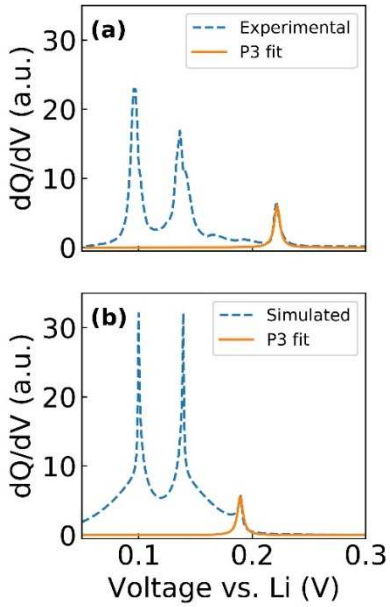


*Figure 8. (a) Experimental result for dQ/dV obtained during delithiation. (b) Simulated result within the 2 layer Bragg-Williams model, obtained with input parameters $\alpha$ = -4.9 kT and $\beta$ = 106. Fitting to the right hand peaks was achieved with a Lorentzian peak in the program Fityk. The resulting peaks possess the same FWHM of 5.8 mV.*

Apart from a small voltage offset in the peak position, which could be attributable to a small deviation from our empirical exponential relationship, equation 6, at the very low lithium occupation of $x_0$ = 0.035, consistency between between the simulations and experimental dQ/dV results is obtained. Therefore the model with $\alpha$ = -4.9 kT and $\beta$ = 106 captures the important physical description of peak P3l/P3d, i.e. the occupation fraction obtained from integration of the peak, and its FWHM.

We now present thermodynamic arguments to explain the formation of the peak. Using well-known thermodynamic relationships

$$FE(x) = -\mu(x) = -\Delta G = -\Delta H + T\Delta S, \quad (12)$$

where $\mu(x)$ is the chemical potential of Li in the host and all other terms have been previously defined. The formation of the features in the voltage profile can be explained in terms of the contrasting effects of the $-\Delta H(x)$ and $T\Delta S(x)$ terms on the voltage profile, i.e. $-\Delta G(x)$. For clarity the simulated results are plotted in Figure 9. Note: in Figure 9, $E_0 = 0$ for ease of comparison of the thermodynamic profiles, allowing the partial molar entropy and enthalpy to be shown on the same energy scale. The two separate entropy and enthalpy terms, at the right hand side of equation 12, are shown in Figure 9a-b, while the simulated voltage profile, i.e. the sum of the entropy and enthalpy components, is shown in Figure 9c-d.. The corresponding d$Q$/d$V$ results are shown in Figure 9e-f. At three points, indicated P1, P2, P3, the slope of $T\Delta S(x)$ exactly opposes that of $-\Delta H(x)$. In the case of P1 and P2, associated with the order/disorder transition, these points occur when the slopes of $-\Delta H(x)$ and $T\Delta S(x)$ are both zero. However, for P3 this point does not exactly coincide with the minimum in $-\Delta H(x)$, because of the continuously varying entropy term with occupation x, as clarified in Figure 9b.

We can therefore explain the thermodynamic origin of the plateau P3 (peak in d$Q$/d$V$) as follows. As we previously highlighted, the partial molar entropy in the region of occupation of peak P3 can be described as an ideal solid solution. Here, the entropic term will always cause the free energy of the system to decrease when more Li is added to the system. Left of the peak maximum, i.e. for $x < x_{0,}$ the varying Li-substrate enthalpy term causes this change to occur even faster with changing $x$, resulting in the sharp decrease in voltage. As $x$ approaches the peak maximum, $x_0$, there is a

competition between the maximum in the partial molar enthalpy and the decrease in free energy driven by increasing partial molar entropy. In other words, in the vicinity of the peak P3, the partial molar enthalpy term temporarily opposes any further increase in occupation, while the partial molar entropy term destabilises the system, favouring further filling of the lattice. The net result of both terms is a plateau in chemical potential, i.e. open circuit voltage, and a peak P3 in d$Q$/d$V$. Thereafter, the partial molar enthalpy term tends to a constant and the standard Langmuir (ideal solid solution) filling of the lattice resumes until the onset of the staging transitions. To a first approximation the peak position $x_0$ is driven only by how fast the Li-substrate interaction changes with occupation ($\beta$) while the amplitude of the peak is affected by the strength of the interaction $\alpha$ as well as by $\beta$, as shown in Figure 7.

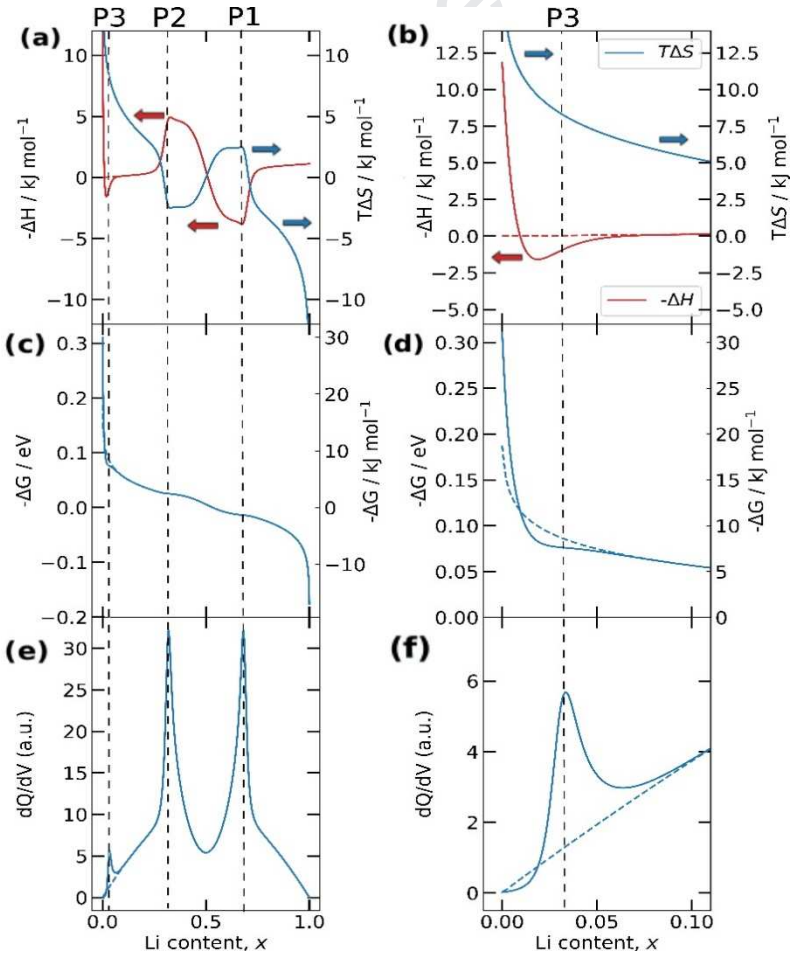

*Figure 9. (a) Left axis: -ΔH(x), right axis TΔS(x), as indicated by arrows, from the two layer Bragg-Williams model with (solid lines) α = -4.9 kT and β = 106; (dashed lines) α = 0 kT and β = 0. (c) Voltage profiles, proportional to -ΔG(x), from direct addition of the two profiles shown in (a). (e) dQ/dV profiles obtained from profile (c). Profiles (b), (d) and (f) correspond to (a), (c) and (e), respectively but over a narrower range of x. Vertical lines indicate the x values of plateaux in voltage (peaks in dQ/dV), and are labelled along the top row.*

## Conclusions

We can model a feature shown in experimental dQ/dV results and voltammograms at low Li occupation, assuming a change in the Li-C interaction at low Li occupation, which has been shown elsewhere to arise from partial charge transfer from Li to the substrate. In contrast with the order/disorder transition associated with the Stage I – Stage II transition at around 50 % Li occupation, the transition at around 7 % Li occupation has a distinct physical origin and does not seem to have any relevance for the partial molar entropy of the system. The latter remains that of an ideal lattice gas.

The physical arguments were supported by a model in which the Li-C interaction was parameterised by an additional correction term with two parameters, in contrast with the usual assumption that this interaction does not vary during intercalation. The values and signs of the parameters were clarified by experimental data, i.e. entropy and enthalpy profiling, and dQ/dV. Although a peak in dQ/dV arises when the interaction term increases or decreases with occupation, the physical interpretation of the model and experimental enthalpy profiles suggest the point term increases with the occupation (i.e. the host lattice becomes less attractive to Li as the occupation increases). In combination with the 2 layer Bragg-Williams model which we previously developed, the complete model permits an evaluation of all the major features observed in electrochemical and

thermodynamic profiles from Li insertion in graphite. We showed that the voltage plateau at low Li occupation, which is associated with a peak in dQ/dV, arises due to the contrasting tendency of the partial molar entropy to favour filling of the lattice and a stabilisation of the system resulting from the varying Li-substrate interaction.

This effect has important ramifications for the modelling of lithium insertion at low Li occupation into graphite. Previous work revealed the effect of cycling in the low Li occupation region on graphitic surface structural damage. Based on theoretical and experimental evidence, we have highlighted in the present article that at low Li occupation in the graphite lattice, dramatic changes occur for the interaction between the adsorbate and the substrate. Thus, models that account for these features are important for describing possible aging induced changes on the relevant profiles in the region of dilute lithium occupation.

We must acknowledge that the present mean field model is still a first-order approximation. In future work we will complement these results with simulations where lithium carbon interaction is considered explicitly. Further, we aim to extend the model to explain the charge/discharge hysteresis observed in the electrochemical profiles during lithiation/delithation in graphite, as a function of different temperatures. In future studies we plan to describe the dynamic behaviour by using the modified Hamiltonian within a kinetic Monte Carlo approach.



Acknowlegments

We thank the Faraday Institution (faraday.ac.uk; EP/S003053/1), grant number FIRG003, for funding. MPM would like to thank the Royal Society of Chemistry for a Researcher Mobility Grant. We thank Richard Fields from University of Manchester Graphene Engineering Innovation Centre for providing the coatings used in the entropy measurements, and Cindy Soares from the

Department of Chemistry at Lancaster University for assisting with the assembly of the coin cells used in the work. EPML acknowledges grants PIP CONICET 11220150100624CO, FONCYT PICT-2015-1605 and SECyT of the Universidad Nacional de Córdoba. Support by CCAD-UNC and GPGPU Computing Group, Y-TEC and an IPAC grant from SNCAD-MinCyT, Argentina, are also gratefully acknowledged. A special thanks to Prof. Rachid Yazami for enlightening discussions which inspired us to pursue the entropy change measurements.

References

[1] E. M. Perassi and E. P. M. Leiva, A theoretical model to determine intercalation entropy and enthalpy: Application to lithium/graphite, *Electrochem. commun.* 65 (2016) 48–52.

[2] M. Otero, A. Sigal, E. M. Perassi, D. Barraco, and E. P. M. Leiva, Statistical mechanical modeling of the transition Stage II → Stage I of Li-ion storage in graphite. A priori vs induced heterogeneity, *Electrochim. Acta* 245 (2017) 569–574.

[3] E. P. M. Leiva, E. Perassi, and D. Barraco, Shedding Light on the Entropy Change Found for the Transition Stage II→Stage I of Li-Ion Storage in Graphite, *J. Electrochem. Soc.* 164 (2016) A6154–A6157.

[4] Y. Reynier, R. Yazami, and B. Fultz, The entropy and enthalpy of lithium intercalation into graphite, *J. Power Sources* 119–121 (2003) 850–855.

[5] D. Allart, M. Montaru, and H. Gualous, Model of Lithium Intercalation into Graphite by Potentiometric Analysis with Equilibrium and Entropy Change Curves of Graphite Electrode, *J. Electrochem. Soc.* 165 (2018) A380–A387.

[6] E. M. Gavilán-Arriazu, O. A. Pinto, B. A. López de Mishima, D. E. Barraco, O. A. Oviedo, and E. P. M. Leiva, The kinetic origin of the Daumas-Hérold model for the Li-ion/graphite intercalation system, *Electrochem. commun.* 93 (2018) 133–137.

[7] C. Sole, N. E. Drewett, and L. J. Hardwick, *In situ* Raman study of lithium-ion intercalation into microcrystalline graphite, *Faraday Discuss.* 172 (2014) 223–237.

[8] R. B. Smith, E. Khoo, and M. Z. Bazant, Intercalation Kinetics in Multiphase-Layered Materials, *J. Phys. Chem. C* 121 (2017) 12505–12523.

[9] M. P. Mercer, S. Finnigan, D. Kramer, D. Richards, and H. E. Hoster, The influence of point defects on the entropy profiles of Lithium Ion Battery cathodes: a lattice-gas Monte Carlo study, *Electrochim. Acta* 241 (2017) 141–152.

[10] E. M. Gavilán Arriazu, B. A. López De Mishima, O. A. Oviedo, E. P. M. Leiva, and O. A. Pinto, Criticality of the phase transition on stage two in a lattice-gas model of a graphite anode in a lithium-ion battery, *Phys. Chem. Chem. Phys.* 19 (2017) 23138–23145.

[11] E. M. Gavilán-Arriazu, O. A. Pinto, B. A. L. de Mishima, E. P. M. Leiva, and O. A. Oviedo, Grand Canonical Monte Carlo Study of Li Intercalation into Graphite, *J. Electrochem. Soc.* 165 (2018) A2019–A2025.

[12] S. Schlueter, R. Genieser, D. Richards, H. E. Hoster, and M. P. Mercer, Quantifying structure dependent responses in Li-ion cells with excess Li spinel cathodes: Matching voltage and entropy profiles through mean field models, *Phys. Chem. Chem. Phys.* 20 (2018) 21417–21429.

[13] J. R. Dahn, Phase diagram of LixC6, *Phys. Rev. B* 44 (1991) 9170–9177.

[14] A. Senyshyn, O. Dolotko, M. J. Muhlbauer, K. Nikolowski, H. Fuess, and H. Ehrenberg, Lithium Intercalation into Graphitic Carbons Revisited: Experimental Evidence for Twisted Bilayer Behavior, *J. Electrochem. Soc.* 160 (2013) A3198–A3205.

[15] S. Taminato *et al.*, Real-time observations of lithium battery reactions - Operando neutron diffraction analysis during practical operation, *Sci. Rep.* 6 (2016) 28843.

[16] N. A. Cañas *et al.*, Operando X-ray diffraction during battery cycling at elevated temperatures: A quantitative analysis of lithium-graphite intercalation compounds, *Carbon* 116 (2017) 255–263.

[17] L. Boulet-Roblin, P. Borel, D. Sheptyakov, C. Tessier, P. Novák, and C. Villevieille, Operando Neutron Powder Diffraction Using Cylindrical Cell Design: The Case of LiNi0.5Mn1.5O4 vs Graphite, *J. Phys. Chem. C* 120 (2016) 17268–17273.

[18] S. Konar, U. Häusserman, and G. Svensson, Intercalation compounds from LiH and graphite: Relative stability of metastable stages and thermodynamic stability of dilute stage Id, *Chem. Mater.* 27 (2015) 2566–2575.

[19] D. Billaud, F. X. Henry, M. Lelaurain, and P. Willmann, Revisited structures of dense and dilute stage II lithium-graphite intercalation compounds, *J. Phys. Chem. Solids*. 57 (1996) 775–781.

[20] V. A. Sethuraman, L. J. Hardwick, V. Srinivasan, and R. Kostecki, Surface structural disordering in graphite upon lithium intercalation/deintercalation, *J. Power Sources* 195 (2010) 3655–3660.

[21] J. R. Dahn, J. N. Reimers, A. K. Sleigh, and T. Tiedje, Density of states in graphite from electrochemical measurements on Lix(C1-zBz)6, *Phys. Rev. B* 45 (1992) 3773–3777.

[22] P. J. Osswald, M. Del Rosario, J. Garche, A. Jossen, and H. E. Hoster, Fast and Accurate Measurement of Entropy Profiles of Commercial Lithium-Ion Cells," *Electrochim. Acta* 177 (2015) 270–276.

[23] M. D. Levi and D. Aurbach, The mechanism of lithium intercalation in graphite film electrodes in aprotic media. Part 1. High resolution slow scan rate cyclic voltammetric studies and modeling, *J. Electroanal. Chem.* 421 (1997) 79–88.

[24] M. D. Levi, C. Wang, J. S. Gnanaraj, and D. Aurbach, Electrochemical behavior of graphite anode at elevated temperatures in organic carbonate solutions, *J. Power Sources* 119–121 (2003) 538–542.

[25] Y. F. Reynier, R. Yazami, and B. Fultz, Thermodynamics of Lithium Intercalation into Graphites and Disordered Carbons, *J. Electrochem. Soc.* 151 (2004) A422-A426.

[26] R. Yazami and Y. Reynier, Thermodynamics and crystal structure anomalies in lithium-intercalated graphite, *J. Power Sources* 153 (2006) 312–318.

[27] K. E. Thomas and J. Newman, Heats of mixing and of entropy in porous insertion electrodes, *J. Power Sources* 119–121 (2003) 844–849.

[28] T. Ohzuku, Formation of Lithium-Graphite Intercalation Compounds in Nonaqueous Electrolytes and Their Application as a Negative Electrode for a Lithium Ion (Shuttlecock) Cell, *J. Electrochem. Soc.* 140 (1993) 2490-2498.

[29] J. -S. Filhol, C. Combelles, R. Yazami, and M. -L. Doublet, Phase Diagrams for Systems with Low Free Energy Variation: A Coupled Theory/Experiments Method Applied to Li-Graphite, *J. Phys. Chem. C* 112 (2008) 3982-3988.

[30] D. P. DiVincenzo and E. J. Mele, Structural Energies in Stage-One Graphite Intercalation Compounds, *Phys. Rev. Lett.* 53 (1984) 52–55.

[31] C. Kittel, *Introduction to Solid State Physics*, Eighth Edit. John Wiley & Sons, Inc., 2005.

[32] A. M. Garay-Tapia, A. H. Romero, and V. Barone, Lithium adsorption on graphene: From isolated adatoms to metallic sheets, *J. Chem. Theory Comput.* 8 (2012) 1064–1071.

[33] F. Valencia, A. H. Romero, F. Ancilotto, and P. L. Silvestrelli, Lithium Adsorption on Graphite from Density Functional Theory Calculations, *J. Phys. Chem. B* 110 (2006) 14832-14841.

[34] E. Lee and K. A. Persson, Li Absorption and Intercalation in Single Layer Graphene and Few Layer Graphene by First Principles, *Nano. Lett.* 12 (2012) 4624-4628.

[35] A. Rakotomahevitra, C. Demangeat, J. C. Parlebas, G. Moraitis, and E. Razafindrakoto, Electronic structure and properties of light atoms intercalated in graphite, *J. Phys. Condens. Matter* 4 (1992) 4621–4632.

[36] H. Tachikawa, Y. Nagoya, and T. Kukuzumi, Density functional theory (DFT) study on the effects of Li+ doping on electronic states of graphene, *J. Power Sources* 195 (2010) 6148-6152.

[37] J. Zheng, Z. Ren, P. Guo, L. Fang, and J. Fan, Diffusion of $Li^+$ ion on graphene: A DFT study, *Appl. Surf. Sci.* 258 (2011) 1651-1655.